# Force-induced wrapping phase transition in activated cellular uptake

Ke Xiao*
*Wenzhou Institute, University of Chinese Academy of Sciences, Wenzhou 325016, People's Republic of China and Department of Physics, College of Physical Science and Technology, Xiamen University, Xiamen 361005, People's Republic of China*

Rui Ma† and Chen-Xu Wu‡
*Fujian Provincial Key Lab for Soft Functional Materials Research, Research Institute for Biomimetics and Soft Matter, Department of Physics, College of Physical Science and Technology, Xiamen University, Xiamen 361005, People's Republic of China*

(Received 17 April 2022; revised 16 August 2022; accepted 3 October 2022; published 26 October 2022)

Intracellular pathogens, including all viruses and many bacteria, enter a host cell through either passive endocytosis or active self-propulsion. Though the cellular uptake of passive particles via endocytic process has been studied extensively, little work has been done on the active entry of self-propelled pathogens, such as *Listeria monocytogenes*. Here, we present a theoretical model to investigate the adhesive wrapping of a self-propelled particle by a plasma membrane, and find a type of first-order wrapping transition from a small partial wrapping state to a large partial wrapping state triggered by the active force. The phase diagram displays more complex behaviors compared with the passive wrapping mediated merely by adhesion. We also find that a tubular protrusion can be formed if the active force exceeds a force barrier. These results may provide a useful guidance to the study of activity-driven cellular entry of active particles into cells.

DOI: 10.1103/PhysRevE.106.044411

## I. INTRODUCTION

Endocytosis is an essential step for a wide range of health related processes [1]. Examples include the transduction of biochemical signal, the intake of nutrients [2,3], and the invasion of pathogens into a cell [4,5] through a plasma membrane, a physical barrier that protects a cell from being infected by pathogens. In order to enter a cell, pathogens can hijack endocytic machineries of the host cell and enter the cell by being wrapped inside the endocytic vesicle through adhesive interactions with the membrane. Extensive studies have been devoted to understanding this adhesion-mediated wrapping process. Theoretical and experimental investigations of such kind have well characterized how the physical parameters, including the particle size [6–12], shape [13–15], elastic properties of the particle [16–20], ligand/receptor density [21–23], as well as the mechanical properties of the membrane [24,25], affect the wrapping behaviors. However, some pathogens such as *Listeria monocytogenes* can generate active force to propel themselves through the plasma membrane by polymerization of actin filaments at its rear body [26–30]. How the active force of these self-propelled agents reshapes the membrane remains to be elucidated.

Active force is an important factor to reshape the membrane. When endocytosis happens in yeast cells, a small patch of membrane is pulled by the actin polymerization force and shaped into a tubular invagination [31–33]. By forming a tether between a bead and a vesicle, a force can be applied on the bead and transmitted to the vesicle. Such experiment is often used to pull a membrane tube from a giant vesicle and measure the elastic properties of the membrane [34–36]. The collective motion of a number of self-propelled particles inside a vesicle were found to induce large deformations of the vesicle [37,38], and even shape transformations [39–41]. Using force to direct particles to pass through a membrane has found a wide range of potential biomedical applications, including drug/gene delivery [42–44], cell operation and manipulation [45,46], and bioimaging/sensing [47,48]. Understanding the role of forces on the interaction between a particle and a membrane is critical to designing efficient strategies for these applications.

To model the action of forces on a membrane, computer simulations are often used with the membrane treated as a collection of particles that make up a mesh, and the movement of the particles is governed by force balance equations [38,49–51]. Another approach to model the action of forces adopts the spirit of continuum mechanics by treating the membrane as a smooth surface and incorporating the work done by the force into the total energy of the membrane [52–54]. By finding the shape that minimizes the total energy, the effect of forces is taken into account [53,54]. In this paper, we choose the second approach and study the membrane deformation under the action of the active force generated by a self-propelled particle. It is found that there exists a force threshold beyond which the membrane starts to wrap around the particle.

*xiaoke@ucas.ac.cn
†ruima@xmu.edu.cn
‡cxwu@xmu.edu.cn

 

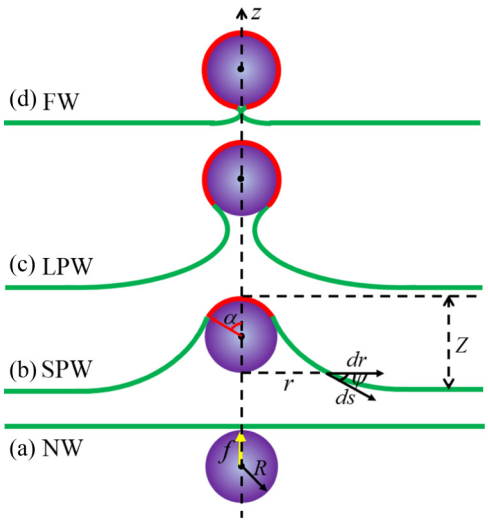


FIG. 1. Schematic of the four different wrapping states: (a) nonwrapping (NW), (b) small partial wrapping (SPW), (c) large partial wrapping (LPW), and (d) full wrapping (FW). The axisymmetric parametrization of the membrane shape is shown in (b). Here, we take the wrapping angle $\alpha$ as an order parameter, and define an SPW state if the wrapping degree is shallow, and an LPW state if the wrapping degree is deep [57].

Further increasing the active force would trigger a first-order transition from a small wrapping state to a large one. Depending on the particle size, the role of the force on the degree of membrane wrapping can be either inhibited for a large particle or promoted for a small particle. It is also found that there exists a force barrier beyond which a tubular structure can be formed on the membrane [53].

## II. THEORETICAL MODELING

Our theoretical model concerns a rigid spherical particle of radius $R$ wrapped by an initially flat membrane. With the work done by the active force included, the total energy of the system is described by the Canham-Helfrich Hamiltonian [8,55,56]

$$E^{\rm tot} = \int_{A_{\rm mem}} \frac{\kappa}{2}(2H)^2 dA + \sigma\,\Delta A - \int_{A_{\rm ad}} \omega\, dA - fZ, \qquad (1)$$

where the first term is the bending energy of the membrane, with bending rigidity $\kappa$ and local mean curvature $H$. The second term is the tension energy, with $\sigma$ being the membrane tension and $\Delta A$ being the excess area, including the wrapped part and the free part of the membrane. The third term represents the gain in adhesive energy, characterized by a negative adhesive energy per unit area $-\omega$, and the last therm arises from the active force $f$ acting on the particle. Here the membrane is pushed by the particle to a height of $Z$, as shown in Fig. 1.

For the spherical particle, the wrapping area generates an adhesive energy of $E_{\rm ad} = -\omega A_{\rm wrapping} = -2\pi\omega R^2(1-\cos\alpha)$. The bending energy of the wrapping part can be written as $E^{\rm ad}_{\rm bend} = 4\pi\kappa(1-\cos\alpha)$. Similarly, the contribution made by the surface tension of the wrapping part can be given explicitly by $E^{\rm ad}_{\rm ten} = \pi\sigma R^2(1-\cos\alpha)^2$, which is proportional to the area difference between the contact area (red in Fig. 1) and the area of its projection. The work done by the active particle for the adhered part is calculated as $E^{\rm ad}_f = -fR(1-\cos\alpha)$. Given these, the energy of the wrapping part reads

$$\frac{E^{\rm tot}_{\rm ad}}{\kappa} = \pi(1-\cos\alpha)\left[\frac{R^2}{\lambda^2}(1-\cos\alpha) - 2\frac{\omega R^2}{\sigma\lambda^2} - \frac{2Rf}{\lambda f_0} + 4\right], \qquad (2)$$

where $\lambda = \sqrt{\kappa/\sigma}$ and $f_0 = 2\pi\sqrt{\kappa\sigma}$ feature a typical length scale and a force scale, respectively.

For the free part of the membrane, its elastic energy comes from the axisymmetrically curved membrane shape described by $r(s)$, $z(s)$ and $\psi(s)$ [see Fig. 1(b)], where $s$ is the arc length of the free membrane. The coordinates $r(s)$ and $z(s)$ depend on $\psi(s)$ through constraints $\dot r = \cos\psi$ and $\dot z = -\sin\psi$, where the dots denote a derivative with respect to the arc length. The total energy of the free membrane, with the two principal curvatures given by $\dot\psi$ and $(\sin\psi)/r$, can be written as [8,56,58]

$$\frac{E^{\rm tot}_{\rm free}}{\kappa} = \pi\int_0^S ds\,\mathcal{L}(\psi,\dot\psi,r,\dot r,\dot z,\eta,\xi,f), \qquad (3)$$

where $\mathcal{L}$ is a Lagrangian defined by

$$\mathcal{L} = r\left(\dot\psi + \frac{\sin\psi}{r}\right)^2 + 2\frac{\sigma}{\kappa}r(1-\cos\psi) - \frac{f}{\pi\kappa}\sin\psi + \eta(\dot r - \cos\psi) + \xi(\dot z + \sin\psi). \qquad (4)$$

Here, $\eta(s)$ and $\xi(s)$ are Lagrangian multipliers to impose the geometric constraints between $r$, $z$, and $\psi$. The term associated with the active force $f$ is proportional to the membrane height of the free part $Z_{\rm free} = \int_0^L \sin\psi\, ds$. A variation of the energy functional Eq. (3) against the shape variables $r(s)$, $z(s)$, and $\psi(s)$ produces a set of shape equations, of which the derivations can be found in the Appendix. Here, we take the value of $\xi$ as a constant which equals to zero due to the fact that its first-order derivative is zero, as well as the variation of the energy against $z(0)$ is zero (see Appendix). With boundary conditions at the contact point between the particle and the membrane, $\psi(0) = \alpha$ and $r(0) = R\sin\alpha$, as well as at the infinity $\psi(\infty) = 0$, and $z(\infty) = 0$, we numerically solve the shape equations for various $\alpha$ and obtain the total energy $E^{\rm tot}(\alpha)$ as a function of the wrapping angle $\alpha$. Based on the optimal wrapping angle $\alpha$ obtained via minimizing the total energy, we identify 4 types of wrapping states: nonwrapping (NW, $\alpha = 0$), small partial wrapping (SPW), large partial wrapping (LPW), and full wrapping (FW, $\alpha = \pi$), as shown in Fig. 1. Such an optimal approach is equivalent to the boundary condition $\dot\psi_0 = 1/R - \sqrt{2\omega/\kappa}$ at the contact line of the free membrane to the spherical surface proved by Ref. [8], where $\dot\psi_0 = d\psi/ds\,|_{s=0}$ is the principal curvature of the free membrane at the contact line along the meridian direction. It should be noted that, in our theoretical model, we consider a special case where the pressure difference between the inside and outside of the plasma membrane, as well as the spontaneous curvature of the membrane, is neglected.

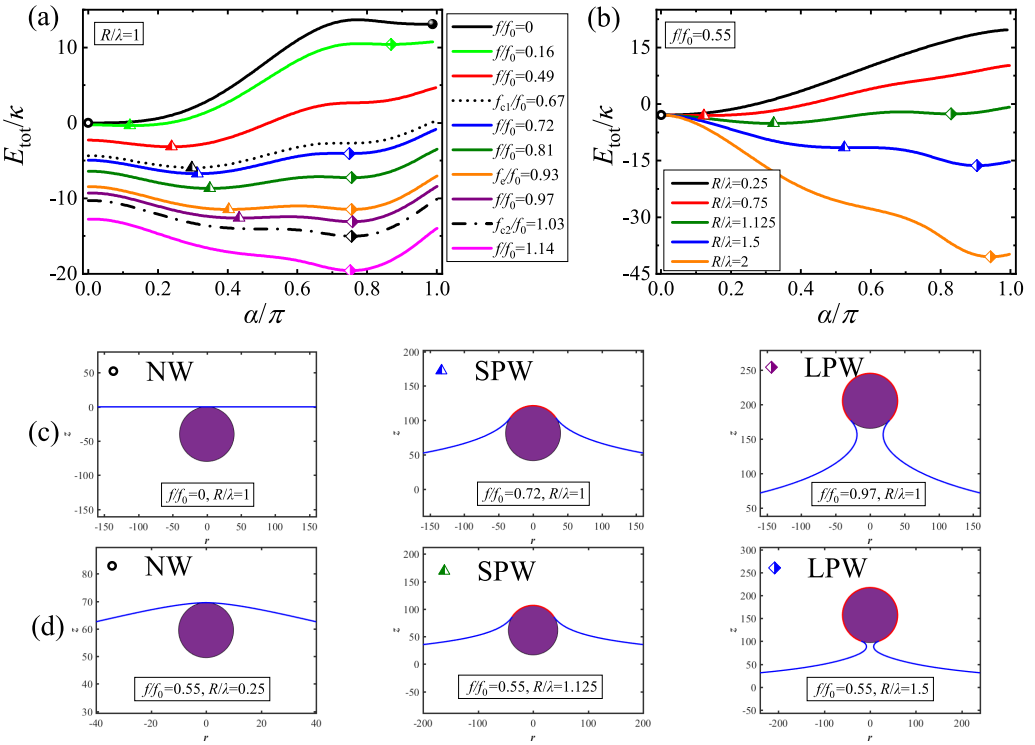


FIG. 2. Total energy profile as a function of wrapping angle with $\omega = 2\sigma$ at (a) fixed $R/\lambda = 1$ and different forces, and (b) fixed force $f/f_0 = 0.55$ and different $R$, respectively. Different wrapping states of the particle for various (c) forces and (d) particle sizes, corresponding to (a) and (b), respectively.

## III. RESULTS AND DISCUSSION

### A. The effect of forces and particle radii on the wrapping states

We numerically solve the shape equations for different wrapping angles $\alpha$ ranging from 0 to $\pi$. Figure 2(a) shows the total energy profile $E_{\rm tot}(\alpha|f)$ as a function of the wrapping angle $\alpha$ for a particle size $R = \lambda$ at different forces $f$. In the absence of active force, there exists a stable NW state and a metastable FW state, corresponding to the empty circle and solid circle, respectively, in the black curve in Fig. 2(a). As $f$ increases, the stable NW state and the metastable FW state shift to a stable SPW state (green and white triangle) and a metastable LPW state (green and white diamond), respectively, as shown by the green curve. Further increase of $f$ results in the disappearance of the LPW state, leaving LPW as the only stable state (see the red and white triangle in the red curve). If the active force $f$ is larger than a certain value $f_{c1}$, a metastable LPW state appears again and the total energy demonstrates two local minima (see the blue curve). If the total energy of the SPW state becomes equal to that of the LPW state at a certain active force $f_e$ (which is the critical first-order transition force), with an energy barrier in between, the two states coexist (see the orange curve). If $f_{c1} < f < f_e$, the SPW state is energetically more favorable (i.e., olive and white triangle in the olive curve), while if $f_e < f < f_{c2}$, the LPW is more favorable (see the purple curve). At active force $f \geqslant f_{c2}$, the SPW-to-LPW energy barrier and the SPW state itself disappear (see the pink curve). A force beyond $f_{c2}$ leads to an LPW state and a tubular structure may form below the particle with a tether radius expected to be smaller than the particle [52].

Besides the active force, the particle size also has a big impact on the wrapping states. Figure 2(b) shows the dependence of wrapping states on particle size. For example, at $f/f_0 = 0.55$, only stable NW state exists for small particle size $R/\lambda = 0.5$ (see black curve). As the particle size increases to $R/\lambda = 0.75$, the stable NW state shifts to stable SPW state (see red curve). A further increase of particle size leads to a metastable LPW state (see the olive curve) besides the stable SPW state. If the particle size goes beyond a threshold value, the metastable LPW state becomes a stable one (see blue curve). If the particle size continues to increase, the metastable SPW state vanishes (see orange curve). Figures 2(c) and 2(d) show 3 typical wrapping states at different combinations of active forces and particle sizes.

### B. Hysteresis in the transition from SPW to LPW

To understand the wrapping behaviors in the regime $f_{c1} \leqslant f \leqslant f_{c2}$, it is of help to plot the optimum wrapping angle $\alpha$ against active force $f$ for different particle sizes, as shown in Fig. 3(a). It is found that the optimum wrapping angle $\alpha$ shows a sharp jump at the critical value $f_e$, a characteristics of first-order transition. Such a transition occurs only for a particle with intermediate sizes with its critical value $f_e$ decreasing monotonically with the particle size, as shown in Fig. 3(b). Plotting the energy barrier $\Delta E/\kappa$ separating the SPW and the LPW states against the critical force $f_e/f_0$ [Fig. 3(c)] exhibits a significantly decreasing behavior. In particular, when $f_e \approx f_0$ and given a typical value of $\kappa = 20\,k_BT$, the energy barrier is only about a few $k_BT$-s, a tiny fraction of the membrane bending rigidity $\kappa$ close to the thermal fluctuation

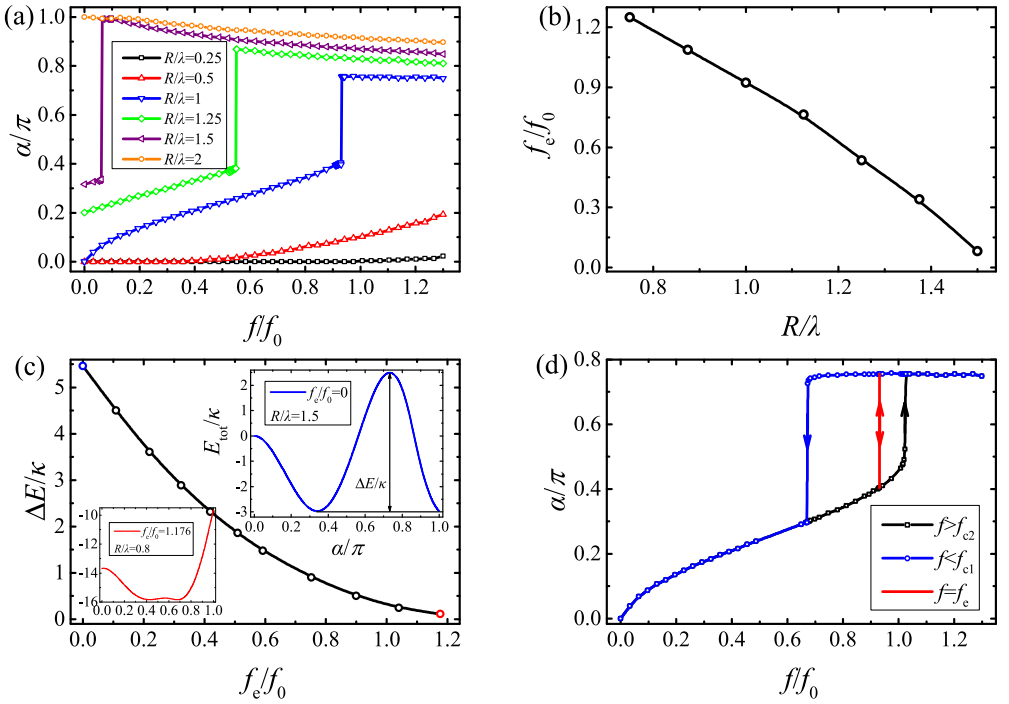


FIG. 3. (a) The dependence of $\alpha$ on $f$ for different particle sizes with $\omega = 2\sigma$. (b) The dependence of the critical force $f_e$ on the particle size. (c) The energy barrier $\Delta E/\kappa$ separating the SPW and the LPW states against the critical force $f_e$. (d) A typical hysteresis associated with $\alpha$ and $f$, with the active force triggering the transition.

energy of membranes. Therefore the first-order transition is plausible. However, if the force is small, the energy barrier of wrapping a particle is too large to be overcome by thermal fluctuations alone. This is consistent with the conclusion of previous studies [8,59]. It is also found that a hysteresis features the transition process, as show in Fig. 3(d).

### C. Phase diagram for force-induced wrapping behaviors

In order to systematically investigate how a wrapping state depends on particle radius $R$ and active force $f$, we construct an $f - R$ phase diagram, as shown in Fig. 4, where four regions of different colors, corresponding to NW, SPW, LPW, and FW states, can be identified. It is found that with increasing active force, the wrapping degree is enhanced from NW to SPW for a small particle, but is reduced from FW to LPW for a large particle. Both of these transitions are continuous. In particular, from NW to SPW, as the membrane remains almost flat ($\psi \ll 1$), it is reasonable to approximate the shape equations to the linear order of $\psi$. Under this approximation, we can obtain an analytical expression for the boundary curve separating NW from SPW, which agrees well with the numerical results, as shown by the red dashed line in Fig. 4. The detailed derivation can be found in the Appendix.

For particle sizes falling in an intermediate range, increasing the active force leads to a discontinuous transition from SPW to LPW, with a sharp jump of the optimum wrapping angle across $\pi/2$. Hysteresis is found to feature the transition with its spinodals shown as dotted ($S_1$) and dash-dotted ($S_2$) curves, respectively. Here, it should be noted that LPW is a novel phase that does not exist in the absence of force.

### D. Force-height relationship for the membrane

To further demonstrate the effect of active force on the membrane shape, we construct the $f-Z$ curve for particles of different radii, which can be obtained by two ways. We first use the force $f$ as the control parameter ($f$-ensemble)

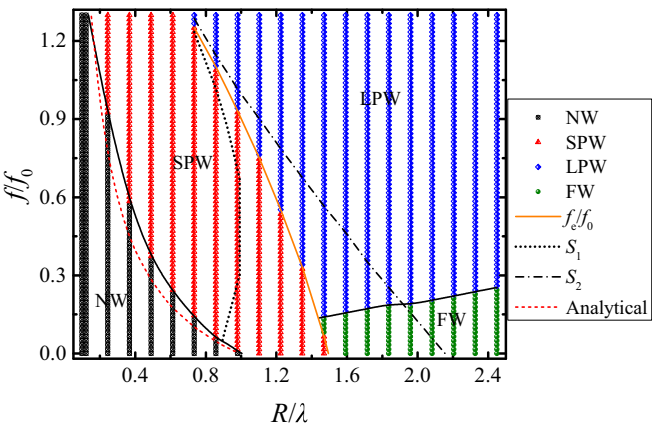


FIG. 4. A two-dimensional wrapping phase diagram on the $(f/f_0 - R/\lambda)$ plane characterizes the interrelated effects of active force and particle size on the cellular uptake, where the ratio between the adhesion and tension strength is given by $\omega/\sigma = 2$. The orange line indicates the discontinuous transition between SPW and LPW. The dotted line and the dash-dotted line indicate the spinodals accompanied with the transition. The black solid lines that separate NW and SPW, and LPW and FW indicate continuous transitions. The red dashed line indicates the analytical solutions for the boundary between NW and SPW.

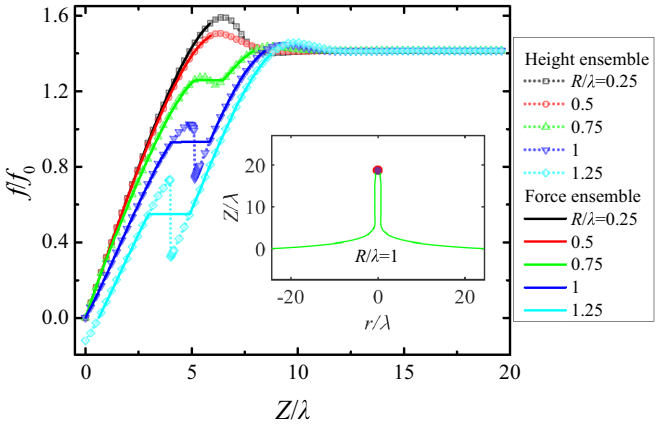


FIG. 5. Active force vs. height curves for different particle sizes. The solid lines and point lines are $f/f_0 - Z/\lambda$ curves for force ensemble and height ensemble, respectively.

to find the optimal wrapping angle $\alpha(f)$ that minimizes the total energy $E^{\text{tot}}(\alpha|f)$, and its corresponding height $Z(f)$. In Fig. 5, the resulting $f-Z$ curves (solid lines) for different particles sizes share similar features to the $f-\alpha$ curves in Fig. 3: there exists an abrupt change of $Z$ at a critical value of active force, indicating that a wrapping transition occurs. We then use the membrane height $Z$ as the control parameter ($Z$-ensemble) to find the solution that minimizes the total energy $E^{\text{tot}}(\alpha|Z)$. The Lagrangian multiplier $f$ to impose the fixed membrane height $Z$ at the optimal wrapping angle is the corresponding force $f(Z)$. Note that the work done by the force is not included in $E^{\text{tot}}(\alpha|Z)$ when calculating the optimal wrapping angle. The resulting $f-Z$ curves (point lines) overlap with those in the $f$-ensemble considerably well in the low membrane height regime. However, with the increase of membrane height $Z$ to the vicinity of the wrapping transition point, the $f-Z$ curves (point lines) deviate from those in the $f$-ensemble (solid lines) through a sharp drop of force, followed by a pickup until a force barrier is formed. The force then smoothly decreases and levels off to a plateau, corresponding to the formation of a tubular structure, as shown in Fig. 5(inset). The force barrier for larger particles is lower than that for smaller particles. However, the plateau force to maintain a tubular shape of membrane is independent of the particle size, a conclusion that has also been reported by Ref. [53]. Here, it should be noted that the occurrence of the plateau is a result of no volume and area constraint in the model [54].

## IV. DISCUSSION

### A. Competition among bending energy, adhesive energy and the work done by the force

We have studied the shape transformations of a flat membrane under the force generated by a self-propelled particle, and shown that a novel phase of LPW appears as a result of the force. The physics behind the transition between different wrapping states comes from the competition among the elastic energy (consisting of bending energy and tension energy), adhesive energy, and the work done by the active force. The calculated total energy, elastics energy (including bending energy and tension energy), adhesive energy, and the work done by active force as a function of wrapping angle are shown in Fig. 6, demonstrating that wrapping is governed by a balance among these energy players. In the absence of force, for a small particle, adhesion-induced wrapping cannot compensate the high energy cost of bending, therefore a NW state is the most stable one. However, the introduction of the work done by the active force reduces the total energy, which enables the membrane to deform and wrap around the particle, even though the wrapping is partial and small due to the little contribution made by adhesion. In contrast, for a large particle ($R \gg \lambda$) at small active force, the FW state is the most stable one because the penalty of elastic energy is sufficiently balanced by adhesive energy. Increasing the force tends to lift up the membrane, which in turn reduces the wrapping degree and consequently leads to a LPW state. Such a transition, according to our theoretical estimation, still exists even at zero adhesive energy, which is consistent with the intuition. In this paper, we choose the adhesion strength $\omega$ such that in the absence of force, increasing the particle size would lead to transition from the SPW state to the FW state.

### B. Biological implications of the phase diagram

For a cell to engulf a self-propelled particle, a FW wrapping state is necessary to enclose the particle inside a vesicle. The phase diagram shown in Fig. 4 suggests that if the particle activity is very strong, it would be difficult for the cell to engulf a very large particle. Instead, the membrane would be pushed into a tubular shape, which is consistent with experimental observations when *Listeria* invades a cell. Once the tube is formed, the force to elongate the tube is not necessarily very large, which has been reported in the work of Derenyi *et al.* [53].

## V. CONCLUSION

In summary, based on the total energy functional, we study the wrapping states of a self-propelled particle when being pushed against a membrane, and find that the active force generated by the particle is able to trigger a first-order wrapping transition, accompanied with a hysteresis behavior. Such a transition provides a deeper insight into the wrapping behaviors induced by a self-propelled particle. The wrapping states of the active particle are tunable by active force and particle size, which can be characterized by a phase diagram in the two-parameter space. We identify that the wrapping degree can be increased (for small particle) or decreased (for large particle) upon enhancing the active force of the particle. A further push of the active particle would lead to the formation of a tubular structure on the cell membrane, a conclusion consistent with previous studies. Our results provide a useful guidance for engineering active particle-based therapeutics and promote biomedical applications.

## ACKNOWLEDGMENTS

We acknowledge financial support from National Natural Science Foundation of China under Grants No. 12147142, No. 11974292, No. 12174323, and No. 12004317,

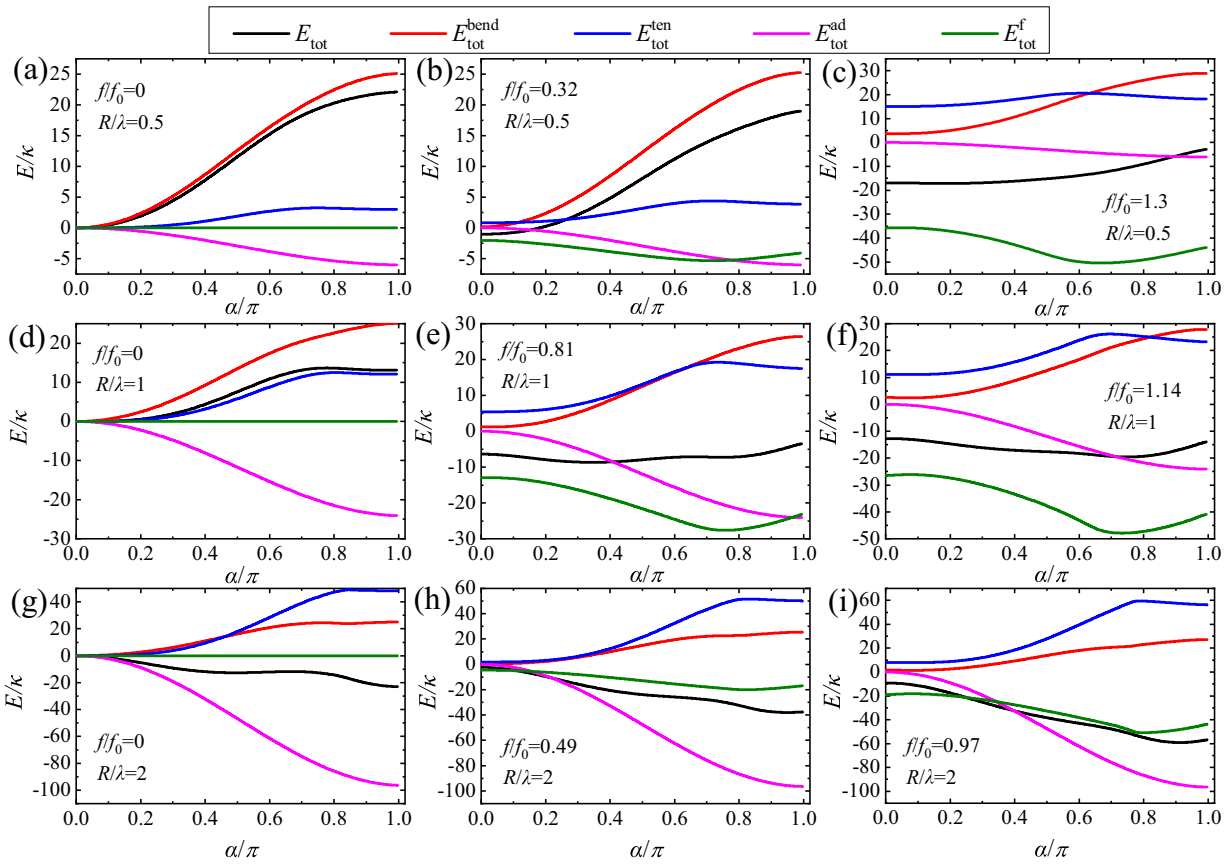


FIG. 6. Energy profile as a function of the wrapping angle for different active forces with $\omega = 2\sigma$. The radius of the particle is set as (a)-(c) $R/\lambda = 0.5$, (d)-(f) $R/\lambda = 1$, and (g)-(i) $R/\lambda = 2$.

Fundamental Research Funds for Central Universities of China under Grant No. 20720200072 (RM), and 111 project No. B16029.

## APPENDIX A: DERIVATION OF THE MEMBRANE SHAPE EQUATIONS

For axisymmetric surfaces, one can derive the Euler-Lagrange equations from the energy functional Eq. (3) in the main text by variational methods:

$$\ddot{\psi} = -\frac{\cos\psi}{r}\dot{\psi} + \frac{\sin\psi\cos\psi}{r^2} + \frac{\sigma}{\kappa}\sin\psi - \frac{f}{2\pi\kappa r}\cos\psi + \frac{\eta}{2r}\sin\psi + \frac{\xi}{2r}\cos\psi, \tag{A1}$$

$$\dot{\eta} = \dot{\psi}^2 - \frac{\sin^2\psi}{r^2} + 2\frac{\sigma}{\kappa}(1-\cos\psi), \tag{A2}$$

$$\dot{\xi} = 0, \tag{A3}$$

$$\dot{r} = \cos\psi, \tag{A4}$$

$$\dot{z} = -\sin\psi, \tag{A5}$$

with corresponding boundary conditions $r(0) = R\sin\alpha$, $\psi(0) = \alpha$, $\psi(\infty) = 0$, and $z(\infty) = 0$. Here the ordinary differential equations along with the boundary conditions are solved in Matlab using 'bvp4c' solver.

Here, we consider a homogeneous membrane, so that the Lagrangian $\mathcal{L}$ is explicitly independent of the arc length $s$. As a result, the Hamiltonian $\mathcal{H} \equiv -\mathcal{L} + \dot{\psi}\partial\mathcal{L}/\partial\dot{\psi} + \dot{r}\partial\mathcal{L}/\partial\dot{r} + \dot{z}\partial\mathcal{L}/\partial\dot{z}$ is a conserved quantity [56] given by

$$\mathcal{H} = r\left(\dot{\psi}^2 - \frac{\sin^2\psi}{r^2}\right) - 2\frac{\sigma}{\kappa}r(1-\cos\psi) + \frac{f}{\pi\kappa}\sin\psi + \eta\cos\psi - \xi\sin\psi. \tag{A6}$$

By combining Eqs. (A1) and (A6), and letting $\xi = 0$, one can derive the general shape equation

$$\ddot{\psi}r^2\cos\psi + \dot{\psi}r\cos^2\psi + \frac{1}{2}\dot{\psi}^2r^2\sin\psi - \frac{1}{2}(\cos^2\psi + 1)\times\sin\psi - \frac{\sigma}{\kappa}r^2\sin\psi + \frac{fr}{2\pi\kappa} = 0. \tag{A7}$$

## APPENDIX B: ANALYTICAL EXPRESSION FOR THE CRITICAL CURVE THAT SEPARATES NW FROM SPW

For weakly deformed membrane ($\psi \ll 1$) and small value of $\alpha$, Eq. (A7) can be linearized as

$$\ddot{\psi}r^2 + \dot{\psi}r - (1+\lambda^{-2}r^2)\psi = -\frac{fr}{2\pi\kappa}. \tag{B1}$$

Here the argument of the function $\psi$ is the radial coordinate $r$, which equals to the arclength $s$ to the first order approximation due to $dr = ds\cos\psi \approx ds + O(\psi^2)$. The general solution of

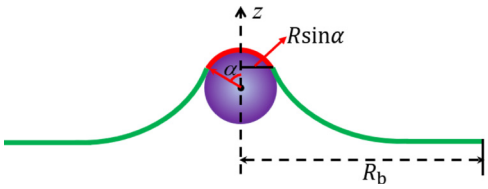


FIG. 7. Definition of some geometric parameters.

this differential equation reads

$$\psi = \frac{f\lambda^2}{2\pi\kappa r} + AI_1(r/\lambda) + BK_1(r/\lambda), \tag{B2}$$

where $I_1(x)$ and $K_1(x)$ are first-order modified Bessel functions, and $A$ and $B$ are integration constants. According to the boundary conditions $\psi(r = R\sin\alpha) = \alpha$ and $\psi(r = +\infty) = 0$, one can determine that $A = 0$ and $B = [\alpha - f\lambda^2/(2\pi\kappa R\sin\alpha)]/K_1(R\sin\alpha/\lambda)$. Therefore, in the limit of $\alpha \ll 1$ and $\psi \ll 1$, we can calculate the work done by the active particle for the free part as

$$E_{\rm f}^{\rm free} = -f\int_{R\alpha}^{R_{\rm b}} \psi \mathrm{d}r$$

$$= -\frac{f\lambda(f\lambda^2 - 2\pi\kappa R\alpha^2)}{2\pi\kappa R\alpha K_1(R\alpha/\lambda)}[K_0(R_{\rm b}/\lambda) - K_0(R\alpha/\lambda)] + \frac{f^2\lambda^2}{2\pi\kappa}\ln\left(\frac{R\alpha}{R_{\rm b}}\right). \tag{B3}$$

Here the lower limit for the integration variable $r$ is $R\sin\alpha \approx R\alpha$ as shown in the schematic Fig. 7. The upper limit $R_{\rm b}$ in practice is chosen to be a finite value to avoid divergence of the integral Eq. (B3) when $R_{\rm b} \to \infty$, but large enough (e.g. $R_{\rm b}/\lambda = 1000$) so that further increasing $R_{\rm b}$ brings little change to the result when calculating the second derivative of the total energy, as discussed later in this subsection. The bending energy of the free part of the membrane reads

$$E_{\rm bend}^{\rm free} = \pi\kappa\int_{R\alpha}^{R_{\rm b}}\left(\dot{\psi} + \frac{\psi}{r}\right)^2 r\mathrm{d}r = \left(\frac{f\lambda^2 - 2\pi\kappa R\alpha^2}{2\sqrt{2\pi\kappa}R\alpha\lambda K_1(R\alpha/\lambda)}\right)^2\left[R_{\rm b}^2(K_0^2(R_{\rm b}/\lambda) - K_1^2(R_{\rm b}/\lambda)) + R^2\alpha^2(K_1^2(R\alpha/\lambda) - K_0^2(R\alpha/\lambda))\right], \tag{B4}$$

and the tension energy is given by

$$E_{\rm tens}^{\rm free} = \pi\sigma\int_{R\alpha}^{R_{\rm b}} r\psi^2\mathrm{d}r = \frac{\sigma}{8\pi\kappa^2\alpha^2R^2K_1^2(R\alpha/\lambda)}\Big\{(f\lambda^2 - 2\pi\kappa R\alpha^2)^2\Big[R_{\rm b}^2\big(K_1^2(R_{\rm b}/\lambda) - K_0^2(R_{\rm b}/\lambda)\big) + R^2\alpha^2\big(K_0^2(R\alpha/\lambda) - K_1^2(R\alpha/\lambda)\big)\Big] - 2\lambda(2\pi\kappa R\alpha^2 - f\lambda^2)K_0(R_{\rm b}/\lambda)\cdot\Big[R_{\rm b}(2\pi\kappa R\alpha^2 - f\lambda^2)K_1(R_{\rm b}/\lambda) + 2fR\alpha\lambda^2K_1(R\alpha/\lambda)\Big] + 2R\alpha(4\pi^2\kappa^2R^2\alpha^4\lambda - f^2\lambda^5)K_0(R\alpha/\lambda)K_1(R\alpha/\lambda) + 2f^2R^2\alpha^2\lambda^4K_1^2(R\alpha/\lambda)\ln\frac{R_{\rm b}}{R\alpha}\Big\}. \tag{B5}$$

Summing these three terms and the total energy for the adhesion part, and doing a Taylor expansion with respect to $\alpha$ to the second order of $\alpha$, leads to

$$E_{\rm tot}/\kappa = -\pi\left(\frac{f}{f_0}\right)^2\left[\frac{R_{\rm b}}{\lambda}K_0(R_{\rm b}/\lambda)K_1(R_{\rm b}/\lambda) + \ln(R_{\rm b}/\lambda) + \gamma - \ln 2\right] + \frac{\pi}{2}\left(\frac{f}{f_0}\right)^2\left(\frac{R}{\lambda}\right)^2\alpha^2\Bigg[\left(\ln\alpha + \frac{R_{\rm b}}{\lambda}K_0(R_{\rm b}/\lambda)K_1(R_{\rm b}/\lambda) + \frac{2}{(f/f_0)(R/\lambda)} + \ln(R/\lambda) + \gamma - \ln 2 - \frac{1}{2}\right)^2 - \left(\frac{R_{\rm b}}{\lambda}K_0(R_{\rm b}/\lambda)K_1(R_{\rm b}/\lambda)\right)^2 - 2\frac{\omega/\sigma}{(f/f_0)^2} + \frac{1}{4}\Bigg], \tag{B6}$$

where $\gamma$ is the Euler Gamma function.

$$\frac{\mathrm{d}(E_{\rm tot}/\kappa)}{\mathrm{d}\alpha} = \pi\left(\frac{f}{f_0}\right)^2\left(\frac{R}{\lambda}\right)^2\alpha\Bigg[2\frac{R_{\rm b}}{\lambda}K_0(R_{\rm b}/\lambda)K_1(R_{\rm b}/\lambda)\left(\ln\alpha + \frac{2}{(f/f_0)(R/\lambda)} + \ln(R/\lambda) + \gamma - \ln 2\right) - 2\frac{\omega/\sigma}{(f/f_0)^2} + \left(\frac{2}{(f/f_0)(R/\lambda)} + \gamma\right)^2 + \left(\ln\alpha + \frac{4}{(f/f_0)(R/\lambda)} + \ln(R/\lambda) + 2\gamma - \ln 2\right)\left(\ln\alpha + \ln(R/\lambda) - \ln 2\right)\Bigg], \tag{B7}$$

The second order derivative of the total energy with respect to $\alpha$

is obtained as

$$\frac{\mathrm{d}^2(E_{\mathrm{tot}}/\kappa)}{\mathrm{d}\alpha^2} = \pi\left(\frac{f}{f_0}\right)^2\left(\frac{R}{\lambda}\right)^2\left[\left(\frac{2}{(f/f_0)(R/\lambda)}+\gamma\right)\left(\frac{2}{(f/f_0)(R/\lambda)}+\gamma+2\right)-2\frac{\omega/\sigma}{(f/f_0)^2}\right.$$
$$+2\frac{R_{\mathrm{b}}}{\lambda}K_0(R_{\mathrm{b}}/\lambda)K_1(R_{\mathrm{b}}/\lambda)\left(\ln\alpha+\frac{2}{(f/f_0)(R/\lambda)}+\ln(R/\lambda)+\gamma+1-\ln 2\right)$$
$$\left.+\left(\ln\alpha+\ln(R/\lambda)-\ln 2\right)^2+2\left(\ln\alpha+\ln(R/\lambda)-\ln 2\right)\left(\frac{2}{(f/f_0)(R/\lambda)}+\gamma+1\right)\right]. \tag{B8}$$

By setting $\mathrm{d}^2(E_{\mathrm{tot}}/\kappa)/\mathrm{d}\alpha^2 = 0$, we can get the analytical solution corresponding to the critical transition line between nonwrapping and small partial wrapping, which is shown by the red dash line in Fig. 4 in the main text. A comparison between the analytical results and the exact numerical results indicates that the approximate expression is remarkably accurate.


[1] R. F. Bruinsma, G. J. L. Wuite, and W. H. Roos, Nat. Rev. Phys. **3**, 76 (2021).
[2] F. Frey, F. Ziebert, and U. S. Schwarz, Phys. Rev. E **100**, 052403 (2019).
[3] G. V. Meer and H. Sprong, Curr. Opin. Cell Biol. **16**, 373 (2004).
[4] G. Bao and X. R. Bao, Proc. Natl. Acad. Sci. USA **102**, 9997 (2005).
[5] S. Zhang, H. Gao, and G. Bao, ACS Nano **9**, 8655 (2015).
[6] M. Deserno and W. M. Gelbart, J. Phys. Chem. B **106**, 5543 (2002).
[7] M. Deserno and T. Bickel, Europhysics Letters (EPL) **62**, 767 (2003).
[8] M. Deserno, Phys. Rev. E **69**, 031903 (2004).
[9] S. Zhang, J. Li, G. Lykotrafitis, G. Bao, and S. Suresh, Adv. Mater. **21**, 419 (2009).
[10] B. D. Chithrani, A. A. Ghazani, and W. C. W. Chan, Nano Lett. **6**, 662 (2006).
[11] J. Agudo-Canalejo and R. Lipowsky, ACS Nano **9**, 3704 (2015).
[12] C. Contini, J. W. Hindley, T. J. Macdonald, J. D. Barritt, O. Ces, and N. Quirke, Commun. Chem. **3**, 130 (2020).
[13] F. Frey, F. Ziebert, and U. S. Schwarz, Phys. Rev. Lett. **122**, 088102 (2019).
[14] K. Yang and Y. Ma, Nat. Nanotechnol. **5**, 579 (2010).
[15] Z. Shen, H. Ye, X. Yi, and Y. Li, ACS Nano **13**, 215 (2019).
[16] X. Yi, X. Shi, and H. Gao, Phys. Rev. Lett. **107**, 098101 (2011).
[17] J. C. Shillcock and R. Lipowsky, Nat. Mater. **4**, 225 (2005).
[18] X. Yi and H. Gao, Phys. Rev. E **89**, 062712 (2014).
[19] A. Verma and F. Stellacci, Small **6**, 12 (2010).
[20] X. Ma, X. Yang, M. Li, J. Cui, P. Zhang, Q. Yu, and J. Hao, Langmuir **37**, 11688 (2021).
[21] H. Yuan, J. Li, G. Bao, and S. Zhang, Phys. Rev. Lett. **105**, 138101 (2010).
[22] H. Yuan and S. Zhang, Appl. Phys. Lett. **96**, 033704 (2010).
[23] T. Wiegand, M. Fratini, F. Frey, K. Yserentant, Y. Liu, E. Weber, K. Galior, J. Ohmes, F. Braun, D.-P. Herten, S. Boulant, U. S. Schwarz, K. Salaita, E. A. Cavalcanti-Adam, and J. P. Spatz, Nat. Commun. **11**, 32 (2020).
[24] J. Agudo-Canalejo and R. Lipowsky, Nano Lett. **15**, 7168 (2015).
[25] H. T. Spanke, R. W. Style, C. François-Martin, M. Feofilova, M. Eisentraut, H. Kress, J. Agudo-Canalejo, and E. R. Dufresne, Phys. Rev. Lett. **125**, 198102 (2020).
[26] J. A. Theriot, T. J. Mitchison, L. G. Tilney, and D. A. Portnoy, Nature (London) **357**, 257 (1992).
[27] J. R. Robbins, A. I. Barth, H. Marquis, E. L. de Hostos, W. J. Nelson, and J. A. Theriot, J. Cell Biol. **146**, 1333 (1999).
[28] T. Chakraborty, Immunobiology **201**, 155 (1999).
[29] F. E. Ortega, E. F. Koslover, and J. A. Theriot, eLife **8**, e40032 (2019).
[30] G. C. Dowd, R. Mortuza, M. Bhalla, H. V. Ngo, Y. Li, L. A. Rigano, and K. Ireton, Proc. Natl. Acad. Sci. USA **117**, 3789 (2020).
[31] M. Kaksonen and A. Roux, Nat. Rev. Mol. Cell Biol. **19**, 313 (2018).
[32] M. M. Lacy, R. Ma, N. G. Ravindra, and J. Berro, FEBS Lett. **592**, 3586 (2018).
[33] R. Lu, D. G. Drubin, and Y. Sun, J. Cell Sci. **129**, 1531 (2016).
[34] G. Koster, A. Cacciuto, I. Derényi, D. Frenkel, and M. Dogterom, Phys. Rev. Lett. **94**, 068101 (2005).
[35] R. Dimova, S. Aranda, N. Bezlyepkina, V. Nikolov, K. A. Riske, and R. Lipowsky, J. Phys.: Condens. Matter **18**, S1151 (2006).
[36] D. Cuvelier, I. Derényi, P. Bassereau, and P. Nassoy, Biophys. J. **88**, 2714 (2005).
[37] H. R. Vutukuri, M. Hoore, C. Abaurrea-Velasco, L. van Buren, A. Dutto, T. Auth, D. A. Fedosov, G. Gompper, and J. Vermant, Nature (London) **586**, 52 (2020).
[38] S. C. Takatori and A. Sahu, Phys. Rev. Lett. **124**, 158102 (2020).
[39] C. Wang, Y.-K. Guo, W.-D. Tian, and K. Chen, J. Chem. Phys. **150**, 044907 (2019).
[40] Y. Li and P. R. ten Wolde, Phys. Rev. Lett. **123**, 148003 (2019).
[41] M. S. E. Peterson, A. Baskaran, and M. F. Hagan, Nat. Commun. **12**, 7247 (2021).
[42] J. Panyam and V. Labhasetwar, Adv. Drug Delivery Rev. **55**, 329 (2003).
[43] X. Xu, S. Hou, N. Wattanatorn, F. Wang, Q. Yang, C. Zhao, X. Yu, H.-R. Tseng, S. J. Jonas, and P. S. Weiss, ACS Nano **12**, 4503 (2018).
[44] W. Wang, Z. Wu, X. Lin, T. Si, and Q. He, J. Am. Chem. Soc. **141**, 6601 (2019).

[45] M. Medina-Sánchez, V. Magdanz, M. Guix, V. M. Fomin, and O. G. Schmidt, Adv. Funct. Mater. **28**, 1707228 (2018).
[46] H. Xie, M. Sun, X. Fan, Z. Lin, W. Chen, L. Wang, L. Dong, and Q. He, Sci. Robot. **4**, eaav8006 (2019).
[47] R. Weissleder, Science **312**, 1168 (2006).
[48] D. Peer, J. M. Karp, S. Hong, O. C. Farokhzad, R. Margalit, and R. Langer, Nat. Nanotechnol. **2**, 751 (2007).
[49] P. Chen, Z. Xu, G. Zhu, X. Dai, and L.-T. Yan, Phys. Rev. Lett. **124**, 198102 (2020).
[50] A. Šarić, and A. Cacciuto, Phys. Rev. Lett. **109**, 188101 (2012).
[51] A. Daddi-Moussa-Ider, B. Liebchen, A. M. Menzel, and H. Löwen, New J. Phys. **21**, 083014 (2019).
[52] F. Brochard-Wyart, N. Borghi, D. Cuvelier, and P. Nassoy, Proc. Natl. Acad. Sci. USA **103**, 7660 (2006).
[53] I. Derényi, F. Jülicher, and J. Prost, Phys. Rev. Lett. **88**, 238101 (2002).
[54] B. Božič, S. Svetina, and B. Zeks, Phys. Rev. E **55**, 5834 (1997).
[55] W. Helfrich, Z. Naturforsch. C **28**, 693 (1973).
[56] F. Jülicher and U. Seifert, Phys. Rev. E **49**, 4728 (1994).
[57] S. Dasgupta, A. Thorsten, and G. Gerhard, Nano Lett. **14**, 687 (2014).
[58] U. Seifert and R. Lipowsky, Phys. Rev. A **42**, 4768 (1990).
[59] S. Dasgupta, A. Thorsten, and G. Gerhard, Soft Matter **9**, 5473 (2013).